Proceedings of Global Power and Propulsion Society
ISSN-Nr: 2504-4400
GPPS Chania24
September 4-6, 2024
www.gpps.global

GPPS-TC-2024-0083

NUMERICAL SIMULATION OF A HIGHLY BENT INTAKE DUCT USING MACHINE LEARNING ALGORITHMS TO CLOSE THE RANS EQUATIONS

Markus Carlos Hein
Institute of Jet Propulsion
University of the Bundeswehr Munich
contact@carlos-hein.com
Neubiberg, Germany

Maximilian Reissmann
Department of Mechanical Engineering
University of Melbourne
reissmannm@student.unimelb.edu.au
Melbourne, Australia

Julian A. Scheibel
Institute of Jet Propulsion
University of the Bundeswehr Munich
julian.scheibel@unibw.de
Neubiberg, Germany

Marcel Stößel
Institute of Jet Propulsion
University of the Bundeswehr Munich
m.stoessel@unibw.de
Neubiberg, Germany

Richard D. Sandberg
Department of Mechanical Engineering
University of Melbourne
richard.sandberg@unimelb.edu.au
Melbourne, Australia

Dragan Kožulović
Institute of Jet Propulsion
University of the Bundeswehr Munich
dragan.kozulovic@unibw.de
Neubiberg, Germany

ABSTRACT

This study intends to improve the numerical flow prediction of highly bent intake ducts by the specific use of machine-learning algorithms for the closure of the Reynolds-Averaged-Navier-Stokes (RANS) equations. A computational fluid dynamics (CFD)-driven machine learning approach utilizing an adapted Gene Expression Programming (GEP) algorithm is applied to approximate and iteratively improve an additional anisotropy stress tensor for the definition of Reynolds stresses. The determined turbulence model candidates are evaluated based on experimentally obtained data of the double s-shaped Military Engine Intake Research Duct (MEIRD). The newly generated non-linear stress models deliver a very promising improvement of the agreement with experimental data of MEIRD. This applies especially to the prediction of a large-scale flow separation and the corresponding position of the reattachment zone, which is significantly improved compared to the baseline k-ω SST model, closely matching the experimentally obtained data. Applying the model to non-trained operating points is shown to achieve similar improvements. Conclusively, the performance of the model is discussed in terms of remaining weaknesses and suggestions for further developments are presented.

INTRODUCTION

The demand for highly bent intake ducts to realise compact engine integration with minimised overall system weight is constantly increasing for military and civil applications. Modern fighter aircraft require a minimised radar signature (Wong et al., 2006), unmanned aerial vehicles (UAVs) call for tight intake designs, blended wing body systems require the air supply of an internal engine (Okonkwo and Smith, 2016) and new civil airframe concepts also point to an increased complexity in engine integration, e.g. in order to realise boundary layer ingestion measures (Hall et al., 2017). Serpentine (s-shaped) ducts address these primarily geometric requirements by avoiding a clear line of sight to the compressor stage, enabling a low-volume intake design and opening up engine mass flow routing with significantly more degrees of freedom compared to the classic axial nacelle design. However, the strong curvature leads to cross-flow centrifugal pressure gradients and tends to promote separation zones (Guo and Seddon, 1983). In combination with counter-rotating vortex pairs that arise at each bend, a mutual pressure and swirl distortion is induced entering the downstream low-pressure compressor. Reducing this engine inflow distortion is a key challenge in the realisation of modern engine integration concepts.

This work is licensed under **Attribution-NonCommercial 4.0 International (CC BY-NC)**
See: https://creativecommons.org/licenses/by-nc/4.0/legalcode

An accurate prediction of these flow distortions is therefore a prerequisite for a reliable design process for future highly bent intakes. However, the modeling of the complex flow conditions is widely reported to still be a very comprehensive challenge for numerical simulation methods. Delot and Scharnhorst (2013) give an overview of different RANS predictions for a circular s-shaped duct including a comparison of different numerical flow solvers and turbulence models. A large divergence of results is demonstrated with a tendency towards improved prediction performance of two-equation models over one-equation and algebraic models, with the models predicting only some of the flow features satisfactorily. The Institute of Jet Propulsion (IJP) has developed an aggressively designed Military Engine Intake Research Duct (MEIRD), which aims at the formation of strong flow distortions in combination with a cross-sectional shape change from a kidney to a circular profile. Numerical results of MEIRD presented by Haug et al. (2019) indicate an asymmetric flow field prediction with a two-equation model, which is not present when using an explicit Reynolds stress model. Berens et al. (2014) report the results of an international study on the application of RANS, unsteady RANS and Detached Eddy Simulation (DES) to a subsonic moderate s-shaped diffuser geometry. The obtained RANS results tend to over-predict the detachment zone, which is reduced by URANS, but is also present in the DES results due to the strong sensitivity to the formation of shear layer instabilities. A strong dynamic behaviour of the distortion coefficients is highlighted, indicating that resolution of unsteady large flow scales is required. Gil-Prieto et al. (2017) confirm this observation by identifying the main dynamic coherent structures within a s-duct featuring a large inclination by comparing delayed DES data and particle image velocimetry data. These findings illustrate the need to apply advanced numerical methods when considering the in-depth dynamic behaviour of highly bent intake ducts. Nevertheless, simultaneously the wide range of applications of s-ducts in future engine integration technologies mentioned encourages additionally an improvement of the flow prediction of classical RANS approaches to keep numerical cost down and design cycles short. This is a key motivation of the present study.

The reported shortcomings of RANS models in predicting separation behaviour of highly bent intake ducts are well known even for canonical test cases such as the periodic hills flow (Breuer et al., 2009; Manceau, 2003). Most RANS turbulence models are based on the Boussinesq hypothesis and assume a linear relation between the Reynolds stress and the mean strain rate. This relation has been shown to be valid only in very limited parts of canonical flows (Schmitt, 2007) and is therefore assumed to be the main cause of RANS uncertainties. Weatheritt and Sandberg (2016) introduced a machine learning approach that relies on Gene Expression Programming (GEP) to add an additional anisotropy tensor to the Boussinesq assumption. This direct development of new RANS closures differs from other recent machine learning implementations that aim at turbulence model parameter fitting by Bayesian methods (Edeling et al., 2014) or the introduction of correction factors e.g. for turbulence production by neural networks (Zhang and Duraisamy, 2015). The GEP framework showed very promising results for canonical flows such as the backward facing step (Weatheritt and Sandberg, 2016) and also for near-application cases such as the wake of a low-pressure turbine cascade (Akolekar et al., 2019). In a modified version that incorporates RANS simulations into the training process, Zhao et al. (2020) demonstrated an improved prediction of the wake mixing process of low- and high-pressure turbine blades.

This study aims to adress the uncertainties in RANS prediction of highly bent intake ducts by the machine-learning driven development of non-linear closures for the anisotropic Reynolds stress. The GEP framework originally introduced by Weatheritt and Sandberg (2016) is applied to simulations of the highly bent MEIRD geometry developed by IJP. The prediction quality of the newly evolved non-linear RANS turbulence models is compared against numerical results based on the $k-\omega$ Shear Stress Transport (SST) model proposed by Menter (1994). The models are tested against experimental MEIRD data under trained and non-trained operating conditions.

EXPERIMENTAL REFERENCE

The Military Engine Intake Research Duct (MEIRD) is a proprietary development of the Institute of Jet Propulsion (IJP), explicitly designed to promote the formation of strong flow distortions representative of highly bent intakes (Rademakers et al., 2016). The experimental data is obtained in the institute's own engine test facility, with the Larzac 04C5

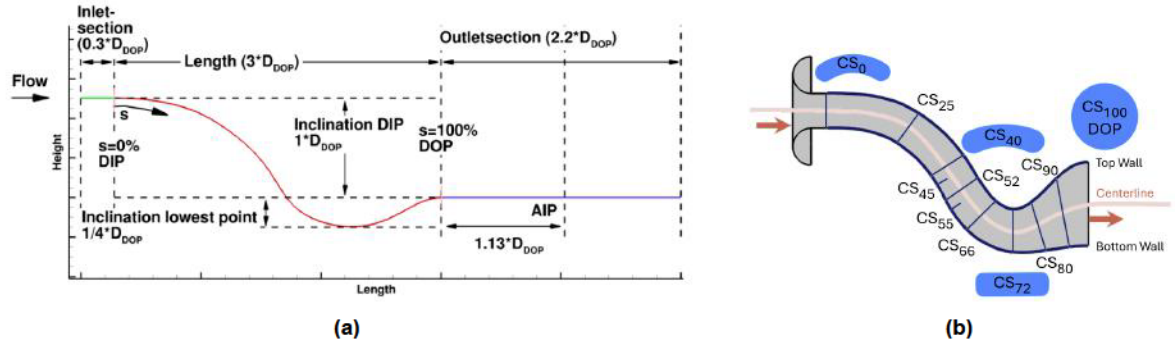

Figure 1 Geometric data and cross-section positioning of MEIRD (Haug et al., 2019)

n_{OP}	$T_{t,in}$	$p_{t,in}$	p_{out}
54%	281.85K	93306Pa	89525Pa
76%	281.6K	93264Pa	84712Pa
86%	281.5K	93255Pa	81563Pa

Table 1 Boundary conditions

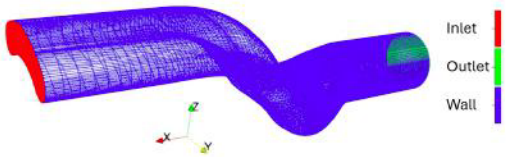

Figure 2 Computational domain of MEIRD

turbofan engine providing the duct mass flow. By placing the Larzac engine directly downstream of the MEIRD or alternatively downstream of an additional mixing tube, the interaction between the engine and the intake can be specifically addressed or suppressed. This study focuses on the internal duct flow and the predictive quality of duct-only simulations and therefore relies on experimental data in a "non-coupled" configuration.

The parameterised shape of the MEIRD centreline is depicted in fig. 1(a). An inclination of one times the diameter of the duct outlet plane $d_{DOP} = 0.454m$ is realized by a double s-shape contour. The duct inlet plane (DIP) at $s = 0\%$ centreline length is located downstream of the bellmouth geometry. In this definition, the part of the centreline marked in red in fig. 1(a) represents the duct itself and the green and blue parts indicate the up-/ downstream extent of the numerical domain, respectively. The cross-sectional shape is based on a kidney profile at the DIP, modifies to a rectangular shape at $s = 72\%$ of the duct centreline length and forms a circular shape at the DOP. In order to achieve a diffusive geometry, the cross-sectional area increases linearly up to the lowest point of the centreline at $s = 72\%$ and remains constant from this position to the DOP with an overall area ratio of $A_{DOP}/A_{DIP} = 1.17$.

Static wall pressure data is available in the duct symmetry plane on the top wall and on the bottom wall. These two data sets are referred to below as centreline top wall and centreline bottom wall. In addition, static pressure probes are distributed at ten cross-sections, as shown in fig. 1(b). The index of the cross-section designations indicates the position along the centreline in percent. A measuring rake equipped with ten kiel probes in radial span and circumferentially traversable in steps of six degrees is located in the aerodynamic interface plane (AIP) and provides total pressure data downstream of the MEIRD. The combination of these experimental data serves as both training set for machine-learning driven turbulence model modification and validation data of new turbulence model candidates.

METHODOLOGY

The study investigates the potential to increase the predictive quality of MEIRD simulations by the targeted use of Gene Expression Programming (GEP) to adjust turbulence models. To enable a comparison between newly developed turbulence model candidates and a two-equation baseline model, the basic numerical settings are kept constant. These general numerical settings are outlined first. Subsequently, the concept of turbulence model fitting by GEP is summarised and explained in detail with respect to the GEP framework settings.

General numerical settings

The numerical analyses are performed with the solver rhoSimpleFoam, which is implemented in the OpenFOAM framework. OpenFOAM is an open-source 3D finite volume code (Weller et al., 1998). All simulations are designed as steady-state, fully turbulent RANS simulations. The divergence terms are discretised by linear upwind methods and the turbulent diffusion is represented by second-order central differentiation. Convergenge is taken to be achieved by a drop of three orders of magnitude of the root mean square residuals of pressure, velocity, energy and turbulent quantities for non-restarted simulations. The two-equation eddy viscosity model $k-\omega\,SST$ proposed by Menter (1994) is used for the reference simulations. The $k-\omega\,SST$ also serves as the basis for the modification of the turbulence model controlled by machine learning. The boundary conditions used for all simulations were derived from the experimental reference case. Total pressure and temperature are defined at the domain inlet and a static pressure condition is prescribed at the outlet. In addition, an axial flow with a moderate turbulence intensity $Tu = 2\%$ is defined. Three different aerodynamic operating conditions are analysed and are listed in Table 1. The specified relative spool speed n_{OP} refers to the Larzac engine providing the duct mass flow and is used to denote the different operating conditions in the remainder of the paper.

The numerical domain is depicted in fig. 2. In contrast to the experimental setup, the bellmouth inlet is not represented. Instead, the numerical domain is extended upstream by the unwound length of the bellmouth in order to still take into account the boundary layer formation within the bellmouth. The domain is spatially discretised by a structured mesh approach following an OH grid structure. The mesh comprises about four million cells and enables the use of wall functions over the entire geometry. The meshing process builds on a grid independence study performed by Haug et al. (2019) as part of a previous numerical MEIRD study.

GEP trained turbulence models

Gene Expression Programming (GEP) belongs to the class of evolutionary algorithms. Based on the cross-generational application of the natural principle of "survival of the fittest", solution candidates (individuals) for an optimisation problem are derived iteratively and non-deterministically. Starting from an initial population, successive generations are formed utilizing genetic operators such as selection, mutation and cross-over. The decisive factor for genetic development is the evaluation of the fitness of the solution candidates based on a problem-specific target criterion. Once the target fitness or the previously defined maximum number of generations has been reached, the process is terminated.

Weatheritt and Sandberg (2016) have introduced a novel GEP framework that enables tensorial regression. This evolutionary algorithm provides an efficient way to apply symbolic regression to a tensor as a target variable. In this study, the GEP framework is used to train an additional anisotropy tensor a_{ij}, which is added to the original linear formulation of the Reynolds stress τ_{ij} of the $k-\omega$ SST model proposed by Menter (1994).

$$\tau_{ij} = \frac{2}{3}\delta_{ij}k - 2\nu_t S_{ij} + a_{ij} \tag{1}$$

As outlined by Pope (1975), the additional anisotropy tensor a_{ij} can be decomposed into a set of tensor bases V_{ij}^k and invariants I_n, which depend on the non-dimensionalised tensors of the strain rate $s_{ij} = S_{ij}/\omega$ and the rotation rate $\omega_{ij} = \Omega_{ij}/\omega$ (ref. to eqn. 2). The number of selected tensor bases is problem-specific and a pre-definition for the GEP trainig setup. For this study, based on experience with previous GEP setups (Zhao et al., 2020), the first three tensor bases and a maximum of the first four invariants according to eqn. 3 are selected.

$$a_{ij} = \sum_k f^{(k)}(I_1, I_2, ..., I_n, N_x) V_{ij}^k \tag{2}$$

$$\begin{aligned} &V_{ij}^1 = s_{ij},\ V_{ij}^2 = s_{ik}\omega_{kj} - \omega_{ik}s_{kj},\ V_{ij}^3 = s_{ik}s_{kj} - \frac{1}{3}\delta_{ij}s_{mn}s_{nm}, \\ &I_1 = s_{mn}s_{nm},\ I_2 = \omega_{mn}\omega_{nm},\ I_3 = s_{km}s_{mn}s_{nk},\ I_4 = \omega_{km}\omega_{mn}s_{nk} \end{aligned} \tag{3}$$

Equation 2 additionally lists flow-related parameters N_x. This is proposed by Fang et al. (2023) in order to enable a higher transferability of the trained turbulence models to related flow cases. Fang et al. (2023) differentiate between free shear flows and wall-bounded flows and define separate parameter sets for each. Due to the consideration of an internal duct flow with significant separation behaviour, the latter are introduced. The remaining functional terms $f^{(k)}$ are the target variables of the GEP training method.

In addition to the implementation of an additional anisotropy tensor a_{ij}, a correction term R is introduced into the original formulation of the turbulence production of the $k-\omega$ *SST* model. Equation 4 specifies the expression for the correction term R as proposed by Schmelzer et al. (2020) including a second tensor b_{ij} which is trained by the GEP framework. The training process is conducted simultaneously to the approximation of a_{ij} and is based on the same choice of invariants I_n, tensor bases V_{ij}^k and flow-related parameters N_x.

$$R = 2kb_{ij}\frac{\partial u_i}{\partial x_j} \quad \leftarrow \quad b_{ij} = \sum_k f^{(k)}(I_1, I_2, ..., I_n, N_x) V_{ij}^k \tag{4}$$

The GEP training process is performed using a CFD-driven approach proposed by Zhao et al. (2020). This approach allows training without information about the Reynolds stress distribution from experimental data or advanced numerical methods by a direct CFD evaluation of the individuals as part of the GEP loop. For each turbulence model candidate (individual), consisting of an expression for a_{ij} and b_{ij}, a RANS simulation is performed during the training process. The quality of the prediction is evaluated by comparing the respective RANS results with experimental data. This is done by means of a cost function, which is used as a selection criterion in the evolutionary process. The cost function of this study is formed from the deviation of the simulation probe data from the experimental MEIRD probe data in the following three subsets: Static pressure at the lower and upper wall centreline ($k = 1$), static pressure at ten cross-sections as depicted in fig. 1 ($k = 2$), total pressure data at the AIP ($k = 3$ / related to eqn. 5).

$$f_{cost,total} = \sum_k (f_{cost,k})^{0.5} \quad \leftarrow \quad f_{cost,k} = \sum_i \frac{(x_{ref,i} - x_{calc,i})^2}{N_{probes}} \tag{5}$$

A comparison of the GEP runs performed with regard to the best fitness achieved by the final turbulence model candidate is summarised in Table 2. All runs feature a population size of 50 individuals iterated over 50 generations. A smaller fitness value indicates a better match with the experimental data. The listing is reduced to the runs differing in GEP framework settings. The best fitness was achieved with a high mutation probability and a consideration of only the first two invariants. Including a corrective expression in the production term of the turbulence kinetic energy transport equation of the $k-\omega$ SST model significantly improved the fitness value. In addition, the use of a language model based memory

function introduced by Reissmann et al. (2024) adapts the initial population according to the specific flow case. Here, this leads to a decrease in convergence time for the optimisation and to a lower fitness for the given number of generations. The prediction quality of the non-linear turbulence model achieving the best fitness value (sixth training run) is evaluated in detail in the result section of this paper. It will be referred to as "Model GEP" in the following.

No.	Scalar invariants	Mutation probability	Reproduction probability	Production term R	Memory function	RANS iterations	Best fitness value
1	I_1,I_2	0.5	0.2	yes	no	200	7050
2	I_1,I_2	0.5	0.2	yes	yes	200	6650
3	I_1,I_2	0.5	0.2	no	no	200	7950
4	I_1,I_2,I_3,I_4	0.5	0.16	no	no	200	7535
5	I_1,I_2,I_3,I_4	0.5	0.16	no	yes	200	7400
6(GEP)	$\boldsymbol{I_1}$,$\boldsymbol{I_2}$	**0.9**	**0.24**	**yes**	**yes**	**200**	**5407**

Table 2 GEP training setups

RESULTS

The prediction quality of the newly evolved "Model GEP" is evaluated by a comparison with calculations based on the reference model $k-\omega$ SST and experimental data from MEIRD. The comparison aims at a performance assessment of the non-linear "Model GEP" under both trained and non-trained operating conditions as a reference for future GEP model training designed for highly bent intake ducts.

Centreline prediction

The entire GEP training process was built on experimental data based on the operating point $n_{OP} = 76\%$ in Table 1. In this sense, $n_{OP} = 76\%$ represents the trained condition and is discussed first. In fig. 3(a), the static centreline pressure at $n_{OP} = 76\%$ calculated with the non-linear "Model GEP" and the reference model $k-\omega$ SST is compared with the experimental measurement. As the pressure distribution at the lower and upper wall is closely coupled, both are shown in a single figure. The data for the upper wall is marked by solid lines and filled circles, the data for the lower wall by dashed lines and unfilled circles.

The experimental data indicate a large-scale flow separation with a clearly assignable plateau in the static pressure distribution on the upper wall. This clear plateau is not visible for the $k-\omega$ SST calculation. In fact, the flow separation is significantly less extensive than in the experiment, which leads to a strong deviation from the experimental reference downstream of the second bend. This shortcoming is significantly improved by the non-linear "Model GEP". The calculated plateau of the static pressure is in close agreement with the experimental data in terms of both geometric position and absolute values of static pressure. In particular, the position of the separation point agrees well, while the axial location of the reattachment is slightly shifted upstream.

The promising improvement of the separation prediction by the use of GEP trained models compared to the reference $k-\omega$ SST model has already been demonstrated for the canonical backward facing step and the periodic hills case (Weatheritt and Sandberg, 2016). The similar behaviour for the MEIRD test case indicates an encouraging transferability of the procedure to three-dimensional internal flows.

Previous numerical studies using the Hellsten EARSM model (Hellsten, 2005) on the MEIRD geometry also covered a resolution of the pressure plateau discussed. This corresponds to the EARSM like character of "Model GEP" in the sense of an anisotropic Reynolds stress representation. However, the absolute value of the static pressure plateau and the position of the reattachment could not be predicted with the Hellsten EARSM model in close agreement with the experiment (Haug et al., 2019), while it is significantly improved by the present "Model GEP".

The distribution of the bottom wall centre pressure is well represented by the $k-\omega$ SST model with a systematic underestimation of the pressure level up to an axial position of $x_{rel} = 0.9$. This discrepancy is also resolved by the GEP trained model.

For the two non-trained operating points, a very similar prediction improvement is achieved with "Model GEP". This applies explicitly both to a reduction of the duct entry Mach number ($n_{OP} = 54\%$ in fig. 3(b)) as well as to an increase ($n_{OP} = 86\%$ in fig. 3(c)). The statements made for the trained operating point can be transferred almost identically to these two operating conditions. In particular, the significant improvement in the prediction of the large-scale flow separation is retained without restriction, with the upstream shifted position of the reattachment remaining the only deficit in identical form.

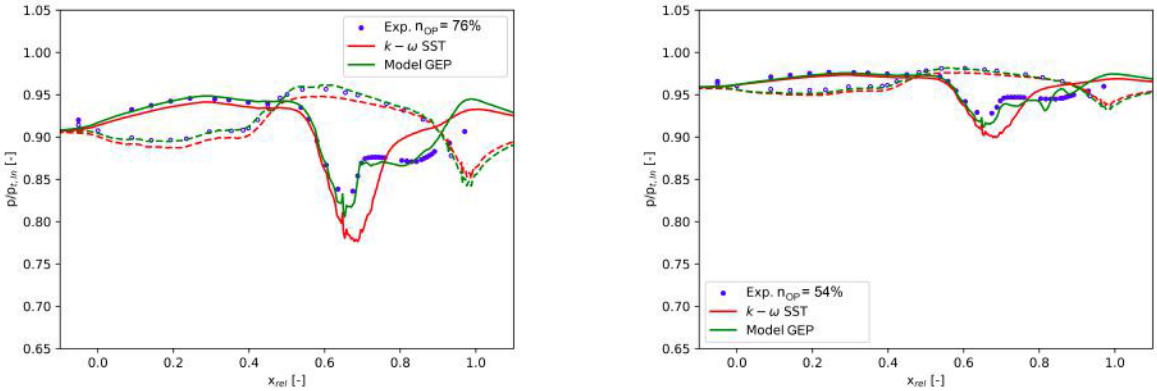

(a) $n_{OP} = 76\%$ (trained)

(b) $n_{OP} = 54\%$ (non-trained)

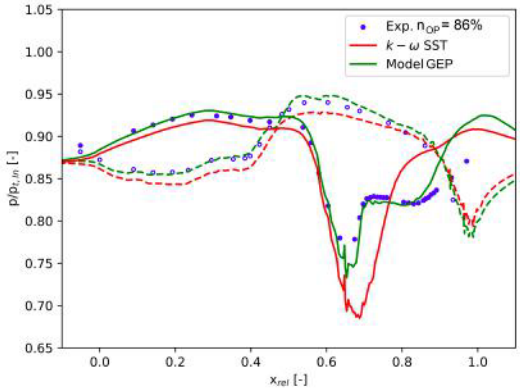

(c) $n_{OP} = 86\%$ (non-trained)

Figure 3 Centreline static wall pressure prediction at trained and non-trained operating conditions

Cross-sectional prediction

Four different cross-sections are selected for the performance evaluation of the non-linear "Model GEP" with regard to the prediction of the static wall pressure along the MEIRD. CS_{25} is located within the first bend, CS_{66} upstream of the second bend, CS_{72} within the second bend and CS_{80} downstream of the second bend. Again, the newly developed "Model GEP" and the reference model $k-\omega$ SST are first compared with experimental MEIRD data under trained operating conditions ($n_{OP} = 76\%$). The comparison is depicted in fig. 4.

For CS_{25} (see fig. 4(a)), both models are in good agreement with the experiment. The slight increase in static pressure by "Model GEP" at the lower wall, which leads to better agreement with the experimental reference, has already been observed for the centreline and also applies in the y-direction (perpendicular to the symmetry plane). Moving downstream to CS_{66}, the discrepancy between $k-\omega$ SST and the experimental values increases with respect to the static pressure at the bottom wall. "Model GEP" continues to predict increased static pressure values compared to $k-\omega$ SST, leading to a better agreement with the experimental reference.

Within the second bend, the discrepancy between the original $k-\omega$ SST model and the experimental data set is most significant. This is plausible as this position is immediately upstream of the separation point, which is not correctly predicted by $k-\omega$ SST. "Model GEP", on the other hand, covers a local pressure maximum close to the symmetry plane at the upper wall in agreement with the absolute experimental values. Note that in contrast to the two previously discussed cross-sections, the lower static pressure level corresponds to the top wall due to the reversal of the geometrical bending direction. It is assumed that the slightly non-uniform shape of the "Model GEP" curve is related to transient effects in connection with the downstream flow separation, which are not resolved in the steady-state approach.

For CS_{80}, the "Model GEP" prediction continues to show the trend of a local pressure maximum, while the experimental data flattens out, leading to a discrepancy similar to the $k-\omega$ SST towards $y = \pm 0.2$. Considering that the training data set contains streamwise distributed static pressure probe data only on the symmetry plane, an improved prediction close to $y = 0$ seems to be explainable. In this sense, additional experimental data on the static wall pressure perpendicular to the symmetry plane might be beneficial for a further improvement of the model.

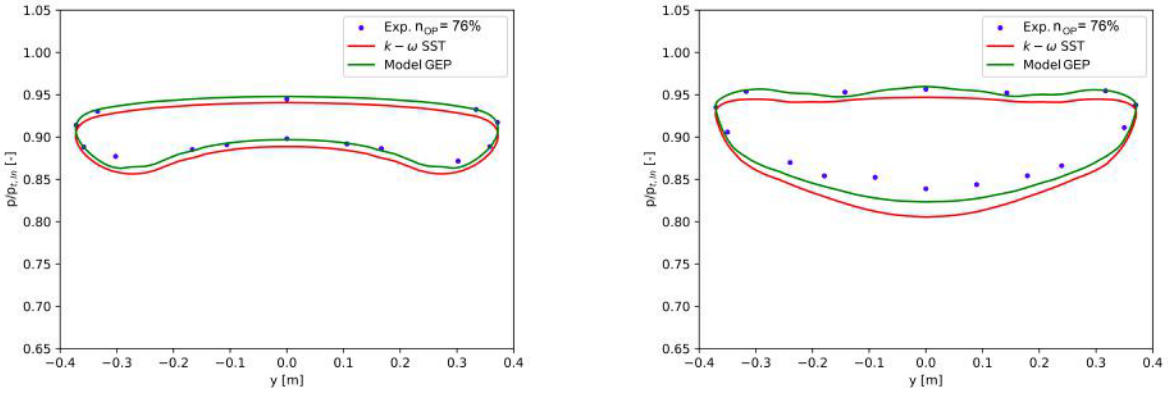

(a) CS_{25} **(b) CS_{66}**

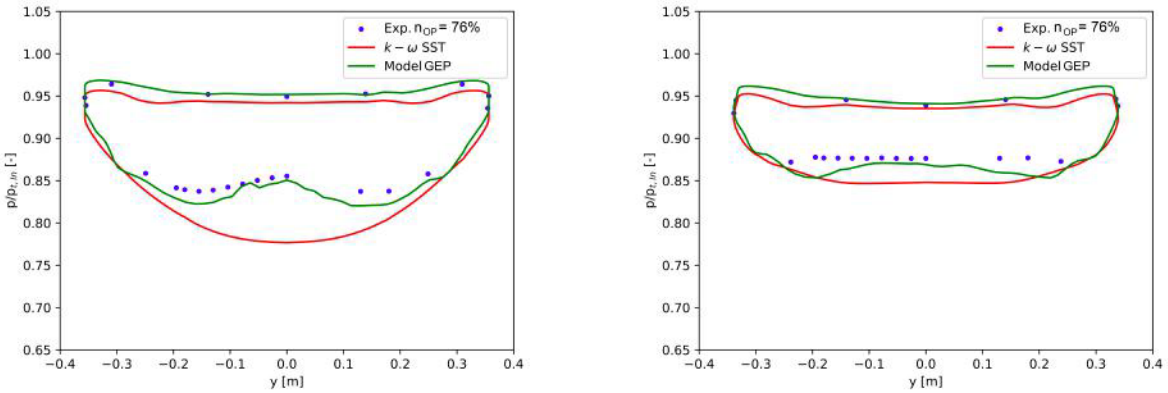

(c) CS_{72} **(d) CS_{80}**

Figure 4 Cross-sectional static pressure distribution at trained operating condition $n_{OP} = 76\%$

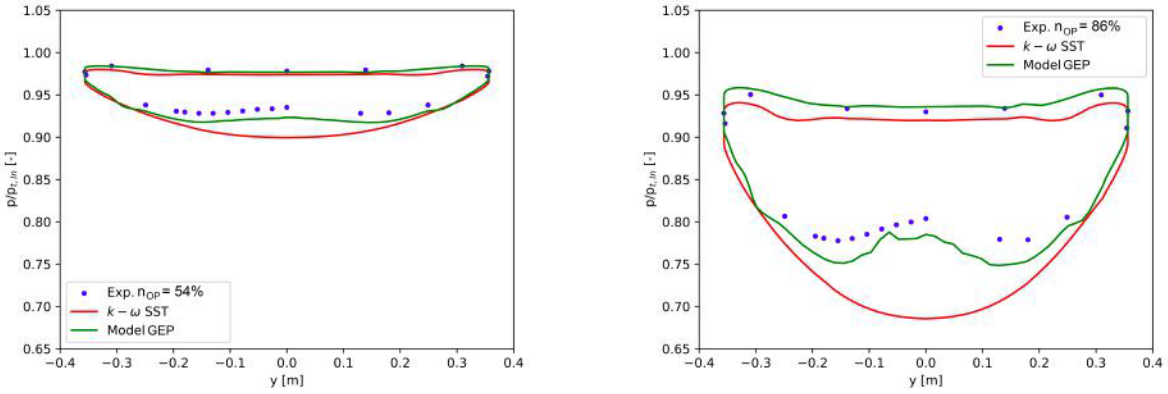

(a) $n_{OP} = 54\%$ **(b) $n_{OP} = 86\%$**

Figure 5 Cross-section CS_{72} static pressure distribution at non-trained operating conditions

The conclusions drawn from the centreline prediction of "Model GEP" under non-trained conditions can be transferred very similarly to the analysis of the cross-sectional pressure distribution. This is demonstrated by fig. 5, which shows the different predictions of the turbulence models in cross-section CS_{72} (largest model deviation in the trained state) for $n_{OP} = 54\%$ and $n_{OP} = 86\%$. For both operating points, the "Model GEP" result behaves like a scaled version of the trained state. This emphasises the applicability of the GEP model independently of the trained operating point, at least for the same geometry.

AIP prediction

A contour plot representation of the MEIRD AIP total pressure distribution calculated with "Model GEP" and the $k-\omega$ SST model is compared with measured data in fig. 6. The trained condition for $n_{OP} = 76\%$ comprises the sub-fig. 6(a)/(c)/(e) (left side from top to bottom). Both numerical models represent the main distortion behaviour of MEIRD, which is characterised by a large total pressure deficit in the upper region due to the large-scale flow separation and a two-part total pressure drop in the lower region, which is amplified by counter-rotating vortex pairs driven by the channel bending. For a detailed description and analysis of the MEIRD flow topology the publications of Haug et al. (2018) and Rademakers et al. (2017) are referred to. The general representation of the expected AIP flow distortions proves that model training on

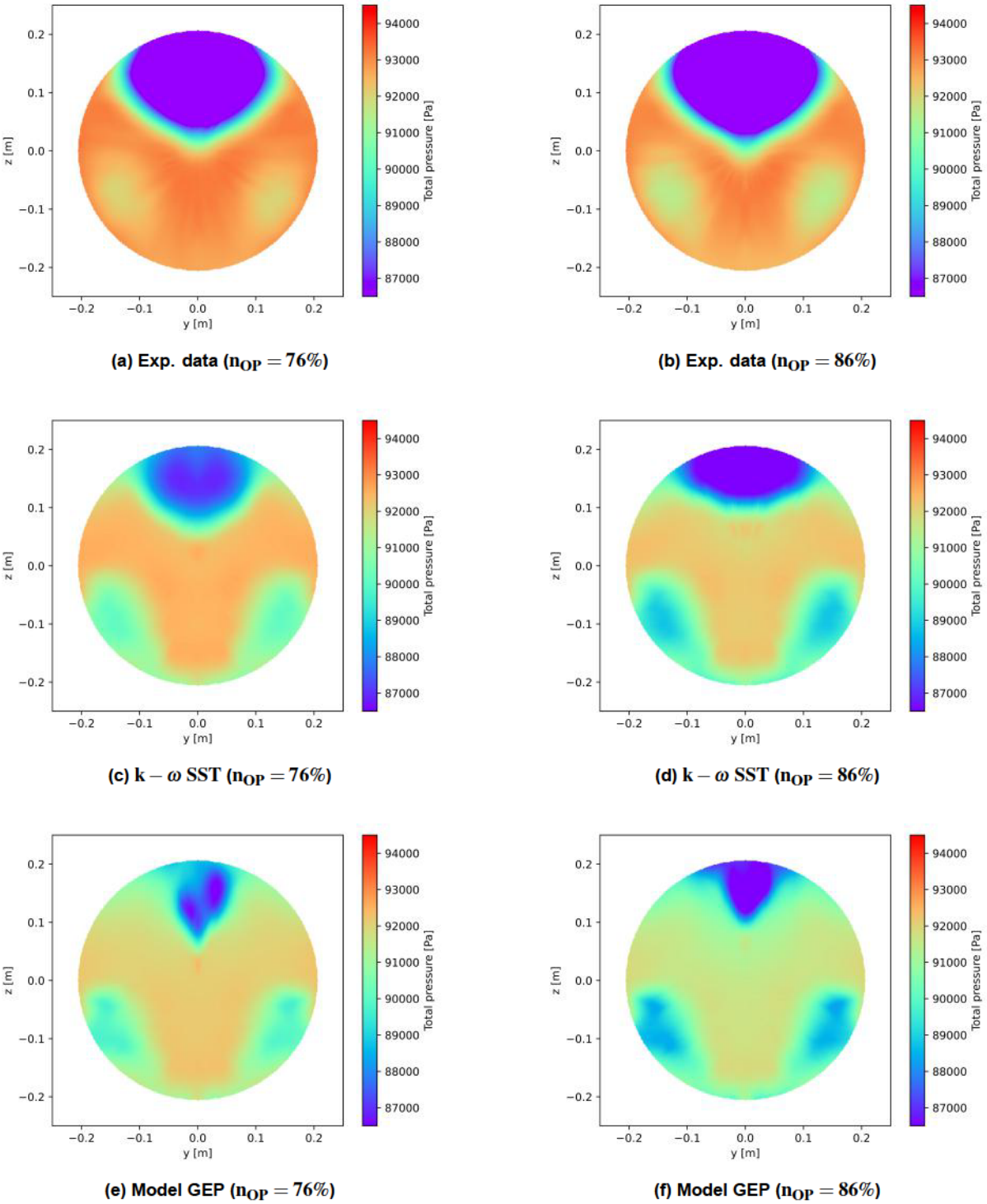

(a) Exp. data ($n_{OP} = 76\%$)

(b) Exp. data ($n_{OP} = 86\%$)

(c) k $-$ ω SST ($n_{OP} = 76\%$)

(d) k $-$ ω SST ($n_{OP} = 86\%$)

(e) Model GEP ($n_{OP} = 76\%$)

(f) Model GEP ($n_{OP} = 86\%$)

Figure 6 Total pressure distribution at AIP at trained operating condition $n_{OP} = 76\%$ (left - (a)/(c)/(e)) and at non-trained operating condition $n_{OP} = 86\%$ (right - (b)/(d)/(f))

Model	p centreline (k=1)	p cross-sections (k=2)	p_t AIP (k=3)	total
k-ω SST	2541	1860	4143	8544
"Model GEP"	763	699	3945	5407

Table 3 Facets of the cost function evaluated for "Model GEP" and the reference model k-ω SST at $n_{OP} = 76\%$

1d probe data points does not lead to an unphysical, non-contiguous shift of the 3d flow prediction. However, in contrast to the evaluation of the centreline and the cross-section calculation, the prediction of "Model GEP" agrees less well with the experimental data than the $k-\omega$ SST model with regard to the shape of the AIP contour. The deviation tendencies of the $k-\omega$ SST model are reflected in a more pronounced form for "Model GEP". Compared to the measured data, the total pressure level of the freestream flow is decreased, while the intensity of the counter-rotating vortex pairs at the bottom is increased. The total pressure defect at the top is compressed in its geometric extent. In addition, "Model GEP" tends to predict an asymmetric formation of this low total pressure region, which is not the case for $k-\omega$ SST. The better agreement of the $k-\omega$ SST model with the experimental data is remarkable at this point, as the causal flow separation is demonstrably not well captured by this model. The deficits in the AIP prediction of the newly evolved Model GEP under trained operating conditions are also found in almost identical form when applied to the non-trained operating point $n_{OP} = 86\%$ (ref. to fig. 6(b)/(d)/(f)). This has already been observed for the centreline and the cross-section prediction. The model behaves predictably and reproducibly with similar strengths and weaknesses under trained and non-trained conditions.

As a measure of the quantitative deviation of the numerical models from the experimental reference data, the evaluated portions of the three facets of the cost function for "Model GEP" and the reference model k-ω SST are listed in Table 3. Reduced values indicate an improvement in the agreement of the simulation result with the experimental reference. For the summation of all three portions (total), a reduction of 35% is achieved by the "Model GEP". In accordance with the previously discussed graphical evaluation, this reduction of the total value can be mainly attributed to the significant improvement of the centreline and the cross-sectional static pressure prediction. In contrast to the evaluation of the shape of the AIP contour plots, the cost function indicates a slight improvement in terms of the averaged deviation from all experimental AIP probe points. However, compared to the centreline and the cross-sectional prediction the AIP deviation remains at a similar level for both models and is to be addressed in future studies.

The experimental training data contains a total of 58 probes distributed along the top and bottom wall centreline, 150 cross-sectional static pressure probes and 341 total pressure probes in the AIP. The evaluated cost function (ref. to eqn. 5) is defined as the summation of the deviation of the numerical solution averaged per data set. Accordingly, the deviation from an experimental data point is finally included in the cost function with a higher weighting, if the corresponding data set contains less validation points. Therefore, the agreement of the simulation results with the centreline measurement data, with the cross-sectional pressure data and with the total pressure data in the AIP is weighted in descending order. This is consistent with the rate of improvement in terms of the prediction quality achieved by "Model GEP". The introduction of targeted weighting expressions into the cost function or alternatively the evaluation of multiple fitness values in terms of a multi-objective training process (Waschkowski et al., 2022) are assumed to be a promising advance, particularly with regard to an improved AIP prediction without the need to expand the training data set.

In terms of an extension of the training data set, currently static wall pressure data distributed along the entire duct length is included, whereas control data for the internal flow determination is available at the AIP only. This implicitly results in a higher weighting of the turbulence model evolution with regard to the wall pressure prediction at main parts of the duct flow. This could be remedied by the acquisition of freestream measurement data at additional streamwise locations.

Training duration

To enable a time efficient and comprehensive variation of the GEP framework settings, a comparatively short training duration was chosen (200 iterations - ref. to Table 2). As a prerequisite for this approach, all training runs were started from a converged solution of the reference model k-ω SST. This procedure is sufficient to achieve the objective of the present study to evaluate the potential of applying the GEP framework to a highly bent intake duct. Though, the training duration may be too short to completely compensate for all transients of the numerical solution. It has been observed that when the "Model GEP" calculations are stopped at the RANS iteration number used within the GEP training loop, the significant improvement over the reference model in terms of the centreline and the cross-sectional prediction is reproducibly achieved. If the calculation time was increased by a factor of five (200 to 1000 iterations), the solutions predicted by the "Model GEP" showed a tendency to evolve again deviations from the experimental reference. This observation is not suitable for generalisation, but is required to be addressed by an extension of the training duration in future studies. In that sense, the development of a final GEP trained model to be published including a specific focus on the convergence behaviour constitutes the conceptual next step based on the presented study. The associated extension of the training duration is considered to be a feasible approach, as it only increases the time required to train the models and there is no time penalty for the aimed application of the models for RANS calculations.

CONCLUSIONS

This paper presented the application of an evolutionary algorithm to develop new non-linear RANS turbulence model closures to improve the flow prediction of highly bent intake ducts. The Gene Expression Programming (GEP) framework proposed by Weatheritt and Sandberg (2016), which enables tensorial regression, was used in a CFD-driven approach. New formulations for an additional anisotropy tensor added to the classical Boussinesq assumption were derived and implemented in the Reynolds stress formulation of the $k-\omega$ SST model. In addition, a correction term for the turbulence production of the $k-\omega$ SST model was determined as part of the identical GEP training loop. The models were trained using experimental data from the double s-shaped Military Engine Intake Research Duct (MEIRD). The newly developed non-linear models showed a significant improvement in the prediction of MEIRD separation behaviour compared to the classical $k-\omega$ SST model. This applies to both the position and the extent of the large-scale flow separation. A comparison with experimental static pressure data at ten cross-sectional positions demonstrated an improvement in wall pressure prediction along the entire duct compared to $k-\omega$ SST. The basic features of the distorted total pressure distribution downstream of the duct outlet were represented by the non-linear models, but in not as good agreement with the experimental reference compared to the original $k-\omega$ SST model. It is assumed that this deficiency is related to the current definition of the cost function, which forms the decisive evaluation parameter for the evolutionary evolvement of the turbulence model candidates. The introduction of weighting factors into this cost function and the transition to an explicit multi-objective training are seen as promising progress aiming at a closer representation of the experimental duct outlet data. The GEP trained model was applied to non-trained operating conditions featuring both an increased and a decreased duct entry Mach number. A very similar and reproducible behaviour as obtained for the trained operating case in terms of prediction quality was demonstrated. In further testing of the GEP trained model, a dependence of the prediction quality on the training duration was observed. For future GEP based training of turbulence models, an extension of the training duration is intended based on the results of the present study.

The improvements achieved by the newly developed non-linear models, especially in wall pressure prediction and separation behaviour, underline a successful transferability of GEP-trained turbulence modelling to highly bent duct flows. The presented study provides a promising basis for future machine-learning driven development of RANS closures aiming at a reliable prediction of engine intake performance under reduced computational effort.

NOMENCLATURE

Latin symbols

A	Area	$[m^2]$
a	Anisotropy tensor	[-]
b	Turbulent production tensor	[-]
d	Diameter	$[m]$
f	Functional expression	[-]
I	Scalar invariant	[-]
k	Turbulence kinetic energy	$[m^2s^{-2}]$
N	Flow related parameter	[-]
n	Spool speed	$[rpm]$
p	Pressure	$[Pa]$
R	Correction term	[-]
s	Strain rate	$[ms^{-1}]$
T	Temperature	$[K]$
Tu	Turbulent intensity	[-]
V	Tensor base	[-]
y^+	Wall distance	[-]

Greek symbols

δ	Kronecker delta	[-]
ν	Eddy viscosity	$[m^2s^{-1}]$
τ	Reynolds stress tensor	[-]
ω	Turbulence dissipation rate	$[m^2s^{-3}]$

Indices

$calc$	Calculated quantity
in	Inflow
i,j,k	Structured order index
op	Operating point
out	Outflow
ref	Reference quantity
rel	Relative quantity
t	Total quantity

References

Akolekar, H. D., Weatheritt, J., Hutchins, N., Sandberg, R. D., Laskowski, G. and Michelassi, V. (2019), 'Development and Use of Machine-Learnt Algebraic Reynolds Stress Models for Enhanced Prediction of Wake Mixing in Low-Pressure Turbines', *Journal of Turbomachinery* **141**(041010). DOI: 10.1115/1.4041753.
URL: *https://doi.org/10.1115/1.4041753*

Berens, T. M., Delot, A.-L., Chevalier, M. and van Muijden, J. (2014), Numerical Simulations for High Offset Intake Diffuser Flows, *in* '52nd Aerospace Sciences Meeting', AIAA SciTech Forum, American Institute of Aeronautics and Astronautics. DOI: 10.2514/6.2014-0371.
URL: *https://arc.aiaa.org/doi/10.2514/6.2014-0371*

Breuer, M., Peller, N., Rapp, C. and Manhart, M. (2009), 'Flow over periodic hills – Numerical and experimental study in a wide range of Reynolds numbers', *Computers & Fluids* **38**(2), 433–457. DOI: 10.1016/j.compfluid.2008.05.002.
URL: *https://www.sciencedirect.com/science/article/pii/S0045793008001126*

Delot, A.-L. and Scharnhorst, R. (2013), A Comparison of Several CFD Codes with Experimental Data in a Diffusing S-Duct, *in* '49th AIAA/ASME/SAE/ASEE Joint Propulsion Conference', American Institute of Aeronautics and Astronautics, San Jose, CA. DOI: 10.2514/6.2013-3796.
URL: *https://arc.aiaa.org/doi/10.2514/6.2013-3796*

Edeling, W. N., Cinnella, P., Dwight, R. P. and Bijl, H. (2014), 'Bayesian estimates of parameter variability in the k–ε turbulence model', *Journal of Computational Physics* **258**, 73–94. DOI: 10.1016/j.jcp.2013.10.027.
URL: *https://www.sciencedirect.com/science/article/pii/S0021999113007031*

Fang, Y., Zhao, Y., Waschkowski, F., Ooi, A. S. H. and Sandberg, R. D. (2023), 'Toward More General Turbulence Models via Multicase Computational-Fluid-Dynamics-Driven Training', *AIAA Journal* **61**(5), 2100–2115. Publisher: American Institute of Aeronautics and Astronautics. DOI: 10.2514/1.J062572.
URL: *https://arc.aiaa.org/doi/10.2514/1.J062572*

Gil-Prieto, D., MacManus, D. G., Zachos, P. K., Tanguy, G., Wilson, F. and Chiereghin, N. (2017), 'Delayed Detached-Eddy Simulation and Particle Image Velocimetry Investigation of S-Duct Flow Distortion', *AIAA Journal* **55**(6), 1893–1908. Publisher: American Institute of Aeronautics and Astronautics. DOI: 10.2514/1.J055468.
URL: *https://doi.org/10.2514/1.J055468*

Guo, R. W. and Seddon, J. (1983), 'The Swirl in an S-Duct of Typical Air Intake Proportions', *Aeronautical Quarterly* **34**(2), 99–129. DOI: 10.1017/S0001925900009641.
URL: *https://www.cambridge.org/core/journals/aeronautical-quarterly/article/abs/swirl-in-an-sduct-of-typical-air-intake-proportions/18C4F91DDB5015D8AAA483FE3D5EA57E*

Hall, D. K., Huang, A. C., Uranga, A., Greitzer, E. M., Drela, M. and Sato, S. (2017), 'Boundary Layer Ingestion Propulsion Benefit for Transport Aircraft', *Journal of Propulsion and Power* **33**(5), 1118–1129. Publisher: American Institute of Aeronautics and Astronautics. DOI: 10.2514/1.B36321.
URL: *https://doi.org/10.2514/1.B36321*

Haug, J. P., Rademakers, R. P., Krummenauer, M. and Niehuis, R. (2019), Validation of RANS simulations of the flow in a short highly bent intake duct, *in* 'Proceedings of the 13th European Conference on Turbomachinery Fluid dynamics and Thermodynamics', Lausanne, Switzerland. DOI: 10.29008/ETC2019-061.
URL: *http://www.euroturbo.eu/publications/proceedings-papers/ETC2019-061/*

Haug, J. P., Rademakers, R. P. M., Stößel, M. and Niehuis, R. (2018), *Numerical Flow Field Analysis in a Highly Bent Intake Duct*, Vol. Volume 2B: Turbomachinery of *Turbo Expo: Power for Land, Sea, and Air*. DOI: 10.1115/GT2018-76633.
URL: *https://doi.org/10.1115/GT2018-76633*

Hellsten, A. (2005), 'New Advanced k-w Turbulence Model for High-Lift Aerodynamics', *AIAA Journal* **43**(9), 1857–1869. Publisher: American Institute of Aeronautics and Astronautics. DOI: 10.2514/1.13754.
URL: *https://doi.org/10.2514/1.13754*

Manceau, R. (2003), 'Report on the 10th joint ERCOFTAC (SIG-15)/IAHR/QNET-CFD Workshop on Refined Turbulence Modelling, Poitiers, october 10-11, 2002', *ERCOFTAC Bulletin* **57**, 11–14. Publisher: European Research Community on Flow, Turbulence And Combustion.
URL: *https://hal.science/hal-02991284*

Menter, F. R. (1994), 'Two-equation eddy-viscosity turbulence models for engineering applications', *AIAA Journal* **32**(8), 1598–1605. Publisher: American Institute of Aeronautics and Astronautics. DOI: 10.2514/3.12149.
URL: *https://arc.aiaa.org/doi/10.2514/3.12149*

Okonkwo, P. and Smith, H. (2016), 'Review of evolving trends in blended wing body aircraft design', *Progress in Aerospace Sciences* **82**, 1–23. DOI: 10.1016/j.paerosci.2015.12.002.
URL: *https://www.sciencedirect.com/science/article/pii/S0376042115300336*

Pope, S. B. (1975), 'A more general effective-viscosity hypothesis', *Journal of Fluid Mechanics* **72**(02), 331. DOI: 10.1017/S0022112075003382.
URL: *http://www.journals.cambridge.org/abstract_S0022112075003382*

Rademakers, R., Kächele, T. and Niehuis, R. (2017), Steady and unsteady flow phenomena in a bent intake duct, *in* 'Proceedings of the 13th International Symposium on Experimental and Computational Aerotherdynamics of Internal Flows, ISAIF13-S-138, Okinawa, Japan'.

Rademakers, R. P. M., Haug, J. P., Niehuis, R. and Stößel, M. (2016), Design and Development of a Military Engine Inlet Research Duct, *in* 'Proceedings of 30th Congress of the International Council of the Aeronautical Sciences, Daejeon, Korea. ICAS2016-0623'.
URL: *https://www.icas.org/ICAS_ARCHIVE/ICAS2016/data/papers/2016_0623_paper.pdf*

Reissmann, M., Fang, Y., Ooi, A. S. H. and Sandberg, R. D. (2024), 'Accelerating evolutionary exploration through language model-based transfer learning'. arXiv:2406.05166 [cs]. DOI: 10.13140/RG.2.2.35600.42240.
URL: *http://arxiv.org/abs/2406.05166*

Schmelzer, M., Dwight, R. P. and Cinnella, P. (2020), 'Discovery of Algebraic Reynolds-Stress Models Using Sparse Symbolic Regression', *Flow, Turbulence and Combustion* **104**(2), 579–603. DOI: 10.1007/s10494-019-00089-x.
URL: *https://doi.org/10.1007/s10494-019-00089-x*

Schmitt, F. (2007), 'About Boussinesq's turbulent viscosity hypothesis: historical remarks and a direct evaluation of its validity', *Comptes Rendus - Mecanique* **335**. DOI: 10.1016/j.crme.2007.08.004.

Waschkowski, F., Zhao, Y., Sandberg, R. and Klewicki, J. (2022), 'Multi-objective CFD-driven development of coupled turbulence closure models', *Journal of Computational Physics* **452**, 110922. DOI: 10.1016/j.jcp.2021.110922.
URL: *https://www.sciencedirect.com/science/article/pii/S0021999121008172*

Weatheritt, J. and Sandberg, R. (2016), 'A novel evolutionary algorithm applied to algebraic modifications of the RANS stress–strain relationship', *Journal of Computational Physics* **325**, 22–37. DOI: 10.1016/j.jcp.2016.08.015.
URL: *https://www.sciencedirect.com/science/article/pii/S0021999116303643*

Weller, H. G., Tabor, G., Jasak, H. and Fureby, C. (1998), 'A tensorial approach to computational continuum mechanics using object-oriented techniques', *Computer in Physics* **12**(6), 620–631. DOI: 10.1063/1.168744.
URL: *https://doi.org/10.1063/1.168744*

Wong, S., Riseborough, E., Duff, G. and Chan, K. (2006), 'Radar cross-section measurements of a full-scale aircraft duct/engine structure', *IEEE Transactions on Antennas and Propagation* **54**(8), 2436–2441. Conference Name: IEEE Transactions on Antennas and Propagation. DOI: 10.1109/TAP.2006.879223.
URL: *https://ieeexplore.ieee.org/document/1668323*

Zhang, Z. J. and Duraisamy, K. (2015), Machine Learning Methods for Data-Driven Turbulence Modeling, *in* '22nd AIAA Computational Fluid Dynamics Conference', American Institute of Aeronautics and Astronautics. DOI: 10.2514/6.2015-2460.
URL: *https://arc.aiaa.org/doi/abs/10.2514/6.2015-2460*

Zhao, Y., Akolekar, H. D., Weatheritt, J., Michelassi, V. and Sandberg, R. D. (2020), 'RANS turbulence model development using CFD-driven machine learning', *Journal of Computational Physics* **411**, 109413. DOI: 10.1016/j.jcp.2020.109413.
URL: *https://www.sciencedirect.com/science/article/pii/S002199912030187X*